

ReFusion: Learning Image Fusion from Reconstruction with Learnable Loss via Meta-Learning

Haowen Bai¹ Zixiang Zhao^{1,2} Jianshe Zhang^{1*} Yichen Wu³
Lilun Deng¹ Yukun Cui¹ Shuang Xu⁴ Baisong Jiang¹

¹ Xi'an Jiaotong University ² Computer Vision Lab, ETH Zürich

³ City University of Hong Kong ⁴ Northwestern Polytechnical University

hwbaii@stu.xjtu.edu.cn, jszhang@mail.xjtu.edu.cn

Abstract

Image fusion aims to combine information from multiple source images into a single and more informative image. A major challenge for deep learning-based image fusion algorithms is the absence of a definitive ground truth and distance measurement. Thus, the manually specified loss functions aiming to steer the model learning, include hyperparameters that need to be manually thereby limiting the model's flexibility and generalizability to unseen tasks. To overcome the limitations of designing loss functions for specific fusion tasks, we propose a unified meta-learning based fusion framework named **ReFusion**, which learns optimal fusion loss from reconstructing source images. **ReFusion** consists of a fusion module, a loss proposal module, and a reconstruction module. Compared with the conventional methods with fixed loss functions, **ReFusion** employs a parameterized loss function, which is dynamically adapted by the loss proposal module based on the specific fusion scene and task. To ensure that the fusion network preserves maximal information from the source images, makes it possible to reconstruct the original images from the fusion image, a meta-learning strategy is used to make the reconstruction loss continually refine the parameters of the loss proposal module. Adaptive updating is achieved by alternating between inter update, outer update, and fusion update, where the training of the three components facilitates each other. Extensive experiments affirm that our method can successfully adapt to diverse fusion tasks, including infrared-visible, multi-focus, multi-exposure, and medical image fusion problems. The code will be released.

1. Introduction

Image fusion is a research area within computer vision and image processing that aims to combine information from multiple images of the same scene into a singular, enriched image. The fusion process leverages the strengths of each source image while mitigating the weaknesses inherent in unimodal imaging or specific imaging techniques, thereby improving the overall quality and utility of the fused image. The core advantage of image fusion lies in its capacity to synthesize information from disparate imaging sources that may differ in sensor type, focus area, or exposure time. Its wide variety of applications span medical imaging [15, 21, 26], remote sensing [4, 63], surveillance and autonomous vehicles [23, 41]. Specifically, infrared-visible image fusion preserves thermal radiation details from infrared images with structural and textural information from visible images. In the medical realm, fusion techniques[57] integrate information from varying modalities, such as MRI and CT scans, offering a more detailed anatomical perspective. Multi-focus image fusion [13, 36, 54, 67] synthesizes fully focused images from pairs of images with distinct focus areas. Similarly, multi-exposure image fusion [39, 40, 66] crafts high dynamic range images from a series of low dynamic range images taken at varying exposure levels.

The lack of ground truth in image fusion necessitates the devising of manually specified loss functions. Predominant practices involve the equal-weighted approximation of the source images [70] within the fused output or the formulation of weighting rules tailored to specific tasks [65] or scene [51]. Additionally, techniques such as adversarial learning have been applied to force the fusion image to closely approximate the source images [37, 38]. Nevertheless, the non-uniform imaging characteristics and information disparities among source images render the application of equal or constant weights for approximation as inherently arbitrary. Weighting strategies based on attributes

*Corresponding author.

like illumination intensity [51] or local information measurement [60, 73] demonstrate a lack of adaptability to the diverse range of tasks and scenarios encountered. Moreover, the simplistic criterion of selecting maximal values from the source images [49, 71] risks the omitting of critical information [52]. Thus, a loss function that can effectively guide different fusion models and is adaptable to multiple scenarios and tasks urgently needs to be proposed.

Meta-learning [11] seeks to enhance the learning algorithms by teaching them the skill of learning, which diverges from the static learning trajectory of conventional algorithms. This adaptive learning approach addresses enduring challenges in deep learning such as data limitations, computational overhead, and the need for improved generalizability. The focal point of optimization in meta-learning typically revolves around parameters [9], optimization algorithms/optimizers [24], and network architectures [27], etc. Within the scope of this paper, we present a novel approach by parameterizing the loss function for image fusion, formulating it through neural networks, and refining it via meta-learning techniques. The resulting adaptive loss function is instrumental in steering the fusion network towards superior performance in image fusion tasks.

The fundamental aim of image fusion is to retain the information present in the source images, with the ideal outcome being a fused image from which the original images can be readily reconstituted [65]. Consequently, reconstruction tasks are frequently employed as an auxiliary to the primary task of fusion [65], with the objective of ensuring the fused image contains attributes that facilitate the reconstruction of the source images. A well-designed fusion loss function should inherently guide the network towards producing a fused image that not only fuses the essential information from source images, but simplifies the task of reconstructing the source images. In light of these considerations, the current paper introduces an innovative image fusion framework. This framework is structured around three core components: a network that proposes loss functions tailored to the specific scenarios and tasks (the adaptive fusion loss proposal module), a streamlined network for effectuating the fusion (the lightweight fusion module), and a two-branch network dedicated to the task of reconstruction (the reconstruction module). The learning process of our framework is divided into three stages as illustrated in Fig. 1, each denoted by the colors red, green, and blue. The inner update represented in red employs the current proposal fusion loss, and the outer update represented in green utilizes the reconstruction loss to measure the effect of the inner update and optimizes the loss proposal module. Lastly, in the fusion and reconstruction update stage, denoted in blue, the fusion module is updated with the proposed fusion loss, and the reconstruction module is updated accordingly. Our main contributions are briefly summarized

as follows:

(1) We introduce ReFusion, a meta-learning based image fusion methodology characterized by a learnable fusion loss function. This function is dynamically generated by a loss proposal module. Remarkably, the module’s learning process proceeds in a meta-learning framework and is solely dependent on the successful reconstruction of the source images, thus circumventing the need for ground truth.

(2) Our approach incorporates a lightweight fusion network architected to fusion features efficiently through interactive feature extraction and gating mechanisms, which guarantees the quality of the fused images with space occupation and computational complexity.

(3) ReFusion achieves high-quality fusion results on various image fusion tasks, including infrared-visible image fusion, multi-focus image fusion, multi-exposure image fusion, and medical image fusion, evidence of the fusion effectiveness and flexibility of our method.

2. Related Work

2.1. DL-based Image Fusion

Deep learning based image fusion methods have revolutionized the field of image fusion by relying on the powerful feature extraction capabilities of neural networks, which can be generally categorized as pixel-level fusion, feature-level fusion and decision-level fusion. Pixel-level fusion combines information from the source image directly from the input image, often leading to enhanced image clarity and spatial resolution. This category also includes GAN-based approach [28, 37] and diffusion based approach [72]. In feature-level fusion, features from the source images are extracted and combined following a specific fusion strategy, and synthesized into a fused image. Predominantly found in autoencoder (AE)-based methods [18, 19, 70, 71], which can be viewed as a deep-learning adaptation of traditional multiscale transform methods [5, 8, 16, 34, 35]. Decision-level fusion methods directly predict decisions or classifications from the source image and interpret and combine the source image into a fused image, which is commonly used in multi-focus image fusion tasks. Some of the work is not limited to the fusion problem itself, combined with image alignment techniques to solve the unaligned source images [14, 61]. Self-supervised learning to train fusion networks without pairs of images [25]. Coupled with high-level visual tasks such as semantic segmentation [31, 47, 48] and object detection [28, 46, 68] to enhance the adaptability of fusion to downstream tasks. The unified model [25, 60, 65] is not limited to specific fusion tasks. In this paper, we address the challenges of lacking ground truth and definitive measurement in image fusion. Instead of employing a fixed loss function, we design a network module to propose an appropriate fusion loss. This

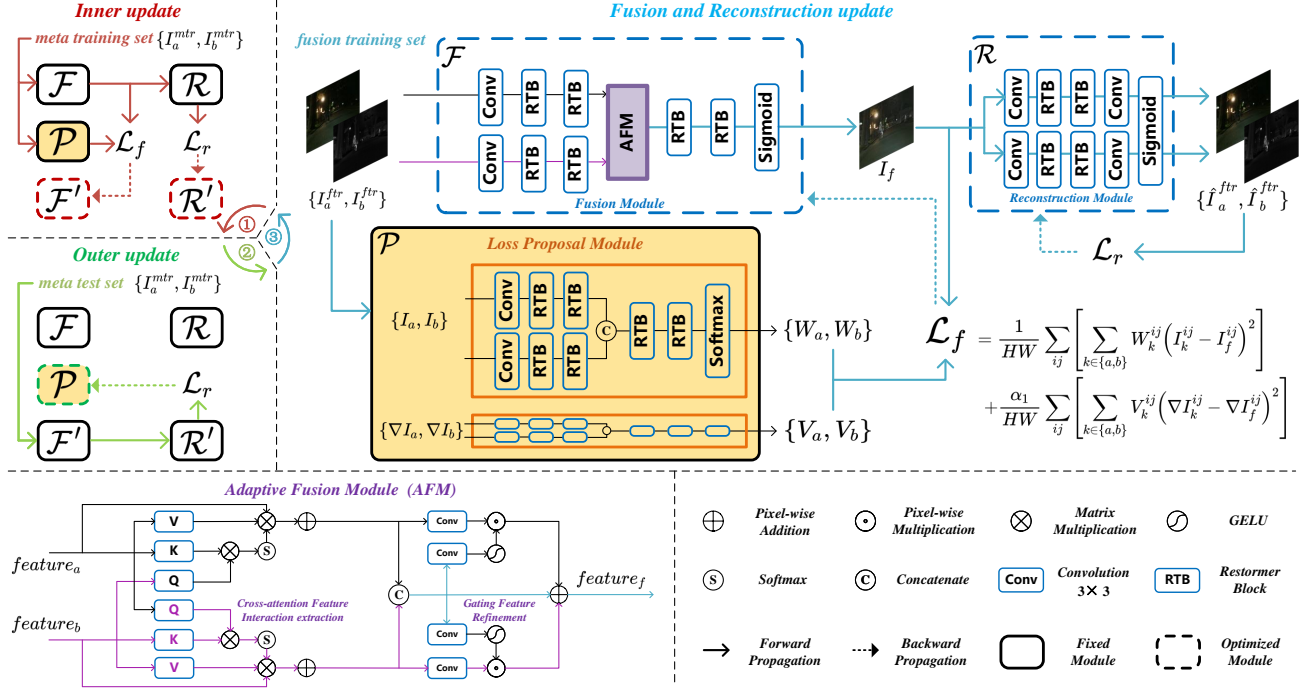


Figure 1. Illustration of Refusion. The alternating three stages are denoted by red, blue, and green, where the inner update denoted by red attempts to update the fusion module using the currently proposed fusion loss, the outer update denoted by green updates the loss proposed module using the reconstruction loss of the meta-test set, and the fusion and reconstruction update stage denoted by blue optimize the fusion module using the proposed fusion loss.

module aims to maximize the retention of information from the source images, updated by reconstruction loss through meta-learning, thus enhancing the efficacy of the fusion process.

2.2. Meta-Learning in Vision

Meta-learning, also known as learning to learn, is a field of research that focuses on developing algorithms to enable models to automatically learn optimal hyperparameters for a given task. It has found widespread applications across various domains. For example, MAML [9] and its variants [10, 42, 43] aim to learn effective model initialization weights, enabling the model to quickly adapt to new tasks with limited examples. Building upon MAML [9], MetaSGD [24] learns the update direction and learning rate for few-shot classification and regression tasks. MW-Net [45] and L2RW [44], on the other hand, focus on learning the important weights of samples using a small, clean validation set to address learning with noisy data problems. Moreover, there are also some works [2, 3, 12] attempt to learn the loss function for better adaptability and generalizability.

In the field of image fusion, Li *et al.* proposes a fusion network that can output an arbitrary resolution, utilizing a learning network to predict filters to achieve an output of artificial scale. Metafusion [68] establishes a mutual pro-

motion algorithm for image fusion and object detection and learns an embedding module for semantic features that is compatible with the fusion features. Liu *et al.* [33] searched for effective network architectures based on fusion mechanisms as well as source image characteristics. In addition, the continuous learning [60] approach focusing on multi-task fusion is also strongly linked to meta-learning. In this work, we concentrate on improving the loss function by parameterizing the preference of the fused image towards the source image within the fusion loss and designing a loss proposed network to learn the parameter of fusion loss in a meta-learning framework. This approach aims to enhance the efficacy of the loss function in guiding the fusion process.

2.3. Comparison with existing approaches

Unlike previous meta-learning based fusion approaches, our work specifically addresses the challenges associated with manually designing fusion losses. This focus represents an effort to refine and automate the process of creating effective fusion loss functions, a key aspect of previous work that often relied on manual intervention. Our methodology distinguishes itself through its learnable loss function, with its parameters proposed by the loss proposal module. This adaptive property allows our loss function to adapt to var-

ious scenarios and tasks. Moreover, while it is common for existing methods to incorporate a reconstruction module within the framework to aid the training of the fusion network, our method employs the reconstruction loss in a novel way. Specifically, the reconstruction loss is used to train the loss proposal module. This is done without affecting the training of the fusion module itself, thus enabling a finer and more autonomous learning process for the fusion network.

3. Method

In this section, the architecture of our framework and its learning mechanism is elucidated. While our method is capable of accommodating multiple image fusion scenarios, for the sake of clarity of exposition, we limit our discussion to the fusion of two source images. Throughout the remainder of this paper, we denote the source images and the fusion image as I_a, I_b and I_f . The reconstructed images corresponding to I_a, I_b are denoted as \hat{I}_a, \hat{I}_b , respectively.

3.1. Overview

As illustrated in Fig. 1, Refusion consists of three components, *i.e.*, the fusion module $\mathcal{F}(\cdot)$, the reconstruction module $\mathcal{R}(\cdot)$ and the loss proposal module $\mathcal{P}(\cdot)$. \mathcal{F}' and \mathcal{R}' act as interim updated versions of \mathcal{F} and \mathcal{R} , and are integral to the subsequent update of \mathcal{P} . Their parameters are symbolized as $\theta_{\mathcal{F}}, \theta_{\mathcal{R}}, \theta_{\mathcal{P}}, \theta_{\mathcal{F}'}$ and $\theta_{\mathcal{R}'}$, respectively.

Three alternating learning stages constitute Refusion's learning process, represented by the colors red, blue, and green in Fig. 1. The dotted boxes signify the modules that are updated in the current stage. The learnable parameterized fusion loss is denoted as \mathcal{L}_f and the explicit formulation of it will be given in the next section. The reconstruction loss denoted by \mathcal{L}_r , is not involved in the update of the fusion module, unlike previous work that utilized reconstruction.

3.1.1 Learnable Parameterized Fusion Loss

The learnable fusion loss function is constructed from two independent pairs outputs produced by the loss proposal module \mathcal{P} , each pair matching the dimensions of the source images. These pairs are derived from \mathcal{P} using both the source images and their gradients, *i.e.*, $\{[W_a, W_b], [V_a, V_b]\} = \mathcal{P}(I_a, I_b, \nabla I_a, \nabla I_b)$, where $W_a^{ij} + W_b^{ij} = 1$ and $V_a^{ij} + V_b^{ij} = 1$, ∇ stands for the sobel operator. The specific formulation of the learnable fusion loss is defined as follows

$$\mathcal{L}_f = \mathcal{L}_f^{int} + \alpha_1 \mathcal{L}_f^{grad} \quad (1)$$

$$\mathcal{L}_f^{int} = \frac{1}{HW} \sum_{ij} \left[\sum_{k \in \{a,b\}} W_k^{ij} (I_k^{ij} - I_f^{ij})^2 \right] \quad (2)$$

$$\mathcal{L}_f^{grad} = \frac{1}{HW} \sum_{ij} \left[\sum_{k \in \{a,b\}} V_k^{ij} (\nabla I_k^{ij} - \nabla I_f^{ij})^2 \right] \quad (3)$$

where α_1 serves as a tuning parameter. \mathcal{L}_f^{int} and \mathcal{L}_f^{grad} are the intensity loss and gradient loss. The weights W_a and W_b dictate the loss function's preference for the intensity information from each source image, whereas V_a and V_b reflect the emphasis placed on the gradient information. These parameters guide the fusion image to selectively extract pertinent information from the source images. Variations in $\theta_{\mathcal{P}}$ result in different sets of W and V , thereby influencing the characteristics of the fusion loss. $\theta_{\mathcal{P}}$ is updated relying on the reconstruction loss in the in-step update, which is described in the next section. The reconstruction loss consists of intensity loss and gradient loss, and the specific formulation is presented as follows:

$$\mathcal{L}_r = \mathcal{L}_r^{int} + \alpha_2 \mathcal{L}_r^{grad} \quad (4)$$

$$\mathcal{L}_r^{int} = \frac{1}{HW} \sum_{ij} \max_{k \in \{a,b\}} \left[(I_k^{ij} - \hat{I}_k^{ij})^2 \right] \quad (5)$$

$$\mathcal{L}_r^{grad} = \frac{1}{HW} \sum_{ij} \max_{k \in \{a,b\}} \left[(\nabla I_k^{ij} - \nabla \hat{I}_k^{ij})^2 \right] \quad (6)$$

where α_2 is a hyperparameter. $\max(\cdot)$ operation is applied on a pixel-wise basis to mitigate imbalances in the reconstruction process, thereby promoting stability during the training phase.

3.2. Fusion from Reconstruction

To fine-tune the guiding abilities of the loss proposal module \mathcal{P} for fusion tasks, we partition the fusion training dataset, denoted by $\{I_a^{ftr}, I_b^{ftr}\}$, into two subsets: a meta-training set $\{I_a^{mtr}, I_b^{mtr}\}$ and a meta-testing set $\{I_a^{mts}, I_b^{mts}\}$. Samples are drawn from these sets and sequentially introduced into the model at designated stages of the training process.

Inner update towards apply \mathcal{L}_f . During the inner update, we attempt to update \mathcal{F} using the fusion loss as defined by the current state of the loss proposal module \mathcal{P} . This process serves to evaluate \mathcal{P} 's current fusion guidance capabilities. The flow of this stage is represented by the color red in the framework diagram. At this point, the meta-training set $\{I_a^{mtr}, I_b^{mtr}\}$ is input into the model, and the fusion network \mathcal{F} undergoes a single update via gradient descent:

$$\theta_{\mathcal{F}'} = \theta_{\mathcal{F}} - \eta_{\mathcal{F}'} \frac{\partial \mathcal{L}_f(I_a^{mtr}, I_b^{mtr}, I_f^{mtr}; W, V)}{\partial \theta_{\mathcal{F}}} \quad (7)$$

Where W and V are the current outputs of \mathcal{P} , they form the fusion loss as parameters. In the update equation, $\eta_{\mathcal{F}'}$ represents the step size used for updating the fusion module. The module \mathcal{F}' acts as a temporary stand-in for \mathcal{F} and updates the parameters from \mathcal{F} following a single update step. Analogously, the reconstruction module \mathcal{R} undergoes a one-step update to transform into \mathcal{R}' :

$$\theta_{\mathcal{R}'} = \theta_{\mathcal{R}} - \eta_{\mathcal{R}'} \frac{\partial \mathcal{L}_r \left(I_a^{mtr}, I_b^{mtr}, \hat{I}_a^{mtr}, \hat{I}_b^{mtr} \right)}{\partial \theta_{\mathcal{R}}}. \quad (8)$$

Outer update towards optimizing \mathcal{P} . The outer update's primary objective is to refine the loss proposal module \mathcal{P} , that is, to enhance the effectiveness of the loss function \mathcal{L}_f in directing the fusion module \mathcal{F} . This stage is represented by the color green in the framework illustration. The modules \mathcal{F}' and \mathcal{R}' , as derived from the inner update, embody the present instructional capacity of \mathcal{P} . The optimal fusion loss should result in a fused image from which the source images can be more readily reconstructed. Therefore, during this step, the meta-test set $\{I_a^{mts}, I_b^{mts}\}$ is utilized, and the parameters $\theta_{\mathcal{P}}$ are updated based on the reconstruction loss \mathcal{L}_r , which is computed using \mathcal{F}' and \mathcal{R}' :

$$\theta_{\mathcal{P}} = \theta_{\mathcal{P}} - \eta_{\mathcal{P}} \frac{\partial \mathcal{L}_r \left(I_a^{mts}, I_b^{mts}, \hat{I}_a^{mts}, \hat{I}_b^{mts} \right)}{\partial \theta_{\mathcal{P}}}, \quad (9)$$

where the gradient $\partial \mathcal{L}_r / \partial \theta_{\mathcal{P}}$ can be calculated as

$$\frac{\partial \mathcal{L}_r}{\partial \theta_{\mathcal{P}}} = \frac{\partial \mathcal{L}_r}{\partial \theta_{\mathcal{F}'}} * \left(-\eta_{\mathcal{F}'} \frac{\partial^2 \mathcal{L}_f \left(I_a^{mtr}, I_b^{mtr}, I_f^{mtr}; W, V \right)}{\partial \theta_{\mathcal{F}} \partial \theta_{\mathcal{P}}} \right). \quad (10)$$

The updated \mathcal{P} module is adept at formulating an enhanced fusion loss function, which, in turn, enables the fusion module to more effectively assimilate comprehensive information from the source images into the fusion image.

Fusion and Reconstruction update. The cyclical process, which involves several iterations of inner and outer updates, establishes a dynamic and efficient mechanism for the enhancement of \mathcal{P} with respect to the current state of \mathcal{F} . In turn, the refined \mathcal{P} is utilized to further train \mathcal{F} . At this juncture, indicated by the color blue, the inputs from the fusion training set $\{I_a^{ftr}, I_b^{ftr}\}$ are processed, and \mathcal{F} and \mathcal{R} undergo updating through the respective application of the fusion loss \mathcal{L}_f and the reconstruction loss \mathcal{L}_r .

$$\theta_{\mathcal{F}} = \theta_{\mathcal{F}} - \eta_{\mathcal{F}} \frac{\partial \mathcal{L}_f \left(I_a^{ftr}, I_b^{ftr}, I_f^{ftr}; \mathcal{P} \right)}{\partial \theta_{\mathcal{F}}}, \quad (11)$$

$$\theta_{\mathcal{R}} = \theta_{\mathcal{R}} - \eta_{\mathcal{R}} \frac{\partial \mathcal{L}_r \left(I_a^{ftr}, I_b^{ftr}, \hat{I}_a^{ftr}, \hat{I}_b^{ftr} \right)}{\partial \theta_{\mathcal{R}}}. \quad (12)$$

Algorithm 1 ReFusion Training Algorithm

Require:

fusion training set $\{I_a^{ftr}, I_b^{ftr}\}$, meta-training set $\{I_a^{mtr}, I_b^{mtr}\}$ and meta-testing set $\{I_a^{mts}, I_b^{mts}\}$.

Ensure:

Fused image I_f .

- 1: Initialize $\theta_{\mathcal{F}}, \theta_{\mathcal{R}}, \theta_{\mathcal{P}}$.
 - 2: **for** $epoch = 1$ **to** L **do**
 - 3: **for** $step = 1$ **to** M **do**
 - 4: % Inner update: apply \mathcal{P}
 - 5: Sample image pair (I_a^{mtr}, I_b^{mtr}) .
 - 6: Calculate the corresponding $(I_f^{mtr}, \hat{I}_a^{mtr}, \hat{I}_b^{mtr})$.
 - 7: Compute $\theta_{\mathcal{F}'}$ and $\theta_{\mathcal{R}'}$ by Eq. (7) and Eq. (8).
 - 8: % Outer update: optimize \mathcal{P}
 - 9: Sample image pair (I_a^{mts}, I_b^{mts}) .
 - 10: Calculate the corresponding $(I_f^{mts}, \hat{I}_a^{mts}, \hat{I}_b^{mts})$.
 - 11: Update $\theta_{\mathcal{P}}$ by Eq. (9).
 - 12: **end for**
 - 13: **for** $step = 1$ **to** N **do**
 - 14: % Fusion update: optimize \mathcal{F} and \mathcal{R}
 - 15: Sample image pair (I_a^{ftr}, I_b^{ftr}) .
 - 16: Calculate the corresponding $(I_f^{ftr}, \hat{I}_a^{ftr}, \hat{I}_b^{ftr})$.
 - 17: Update $\theta_{\mathcal{F}}$ and $\theta_{\mathcal{R}}$ by Eq. (11) and Eq. (12).
 - 18: **end for**
 - 19: **end for**
-

The training of the fusion framework proceeds through a sequence of alternating stages, each designed to calibrate the fusion loss optimally for the network's current state. This systematic alternation ensures that the fusion network is trained to utilize the most appropriate fusion loss at each stage of its evolution. The culmination of this process is the realization of a highly effective fusion network, finely adjusted for performance. The entire training protocol is detailed in the algorithm presented in Algorithm 1. Due to space constraints, further theoretical understanding of this algorithm is provided in the supplementary material.

Architecture. The structure of ReFusion is shown in Fig. 1. The Restormer Block (RTB) utilizes channel-dimensional self-attention operations to extract features from images, the structure of which can be found in the original paper [64] or in the supplementary material. Within the fusion module, TB is responsible for separating the unique information from the source image and composite fusion image from the fusion features, which are the product of the Adaptive Fusion Module (AFM). The AFM operates by initially employing cross-attention to facilitate interactive feature extraction from the source images. Subsequent to feature concatenation, it utilizes a gating mechanism to refine the unique features of the source images and integrate them into fusion features.

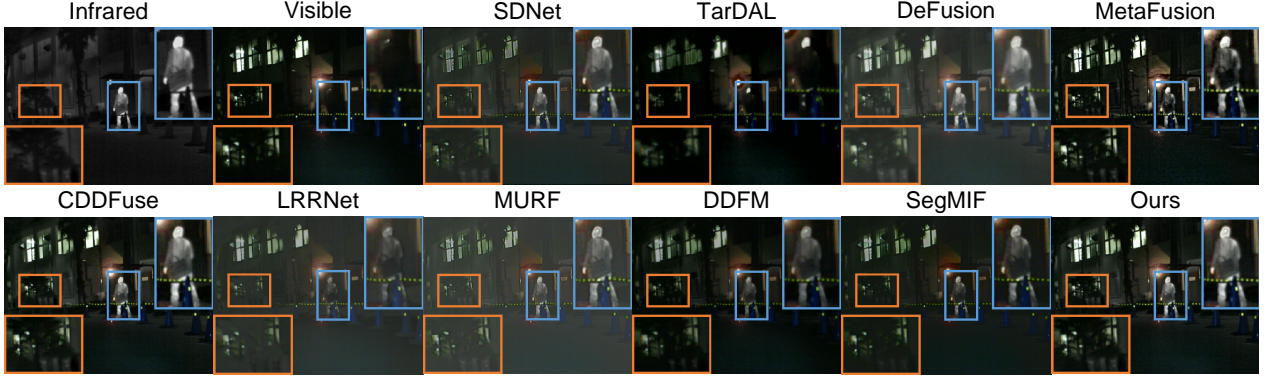


Figure 2. Visual comparison for “00984N” in MSRS dataset.

Infrared-visible image fusion on MSRS [50]							Infrared-visible image fusion on RoadScene [58]						
	EN \uparrow	SD \uparrow	SF \uparrow	AG \uparrow	SCD \uparrow	SSIM \uparrow		EN \uparrow	SD \uparrow	SF \uparrow	AG \uparrow	SCD \uparrow	SSIM \uparrow
SDNet [65]	5.25	17.35	8.67	2.67	0.99	0.36	SDNet [65]	7.10	38.93	12.66	4.91	1.42	<u>0.72</u>
TarDAL [28]	5.28	25.22	5.98	1.83	0.71	0.24	TarDAL [28]	7.11	43.13	9.60	3.43	1.47	0.71
DeFusion [25]	6.46	37.63	8.60	2.80	1.35	0.47	DeFusion [25]	7.23	43.38	9.38	3.68	1.68	0.69
MetaFusion [69]	5.65	24.97	9.99	3.40	1.14	0.18	MetaFusion [69]	6.70	28.59	12.43	4.72	0.93	0.66
CDDFuse [71]	<u>6.70</u>	43.38	<u>11.56</u>	<u>3.73</u>	<u>1.62</u>	<u>0.50</u>	CDDFuse [71]	<u>7.28</u>	<u>44.43</u>	<u>14.10</u>	<u>5.13</u>	<u>1.69</u>	0.70
LRRNet [20]	6.19	31.78	8.46	2.63	0.79	0.22	LRRNet [20]	7.02	37.15	9.87	3.69	1.56	0.62
MURF [62]	5.04	16.37	8.31	2.67	0.86	0.29	MURF [62]	6.80	31.10	12.96	4.88	1.16	0.71
DDFM [72]	6.19	29.26	7.44	2.51	1.45	0.45	DDFM [72]	7.09	38.46	9.11	3.46	1.67	0.71
SegMIF [30]	5.95	37.28	11.10	3.47	1.57	0.35	SegMIF [30]	7.15	42.11	12.31	4.54	1.57	0.59
ReFusion (Ours)	6.71	<u>42.89</u>	11.64	3.80	1.67	0.51	ReFusion (Ours)	7.28	45.65	14.20	5.23	1.70	0.72

Table 1. Quantitative results of infrared-visible image fusion. Best and second-best values are **highlighted** and underlined.

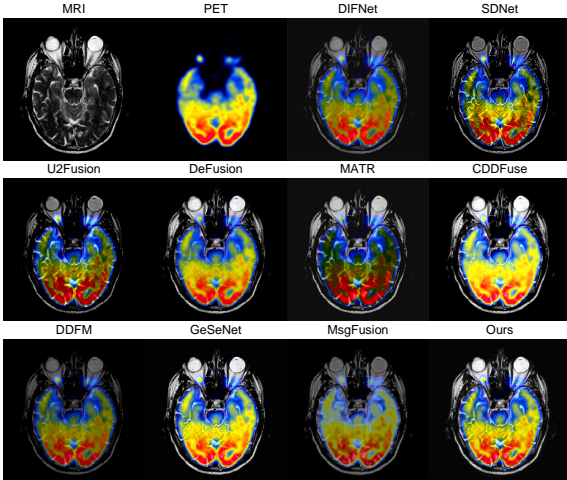


Figure 3. Visualization of the MRI-PET in Harvard Dataset

4. Experiment

4.1. Setup

Throughout the training phase for all tasks, we standardized the number of epochs L at 50, with M and N designated as 600 and 1622, respectively. We utilize Adam optimizer, initiated with a learning rate of $1e-4$. During the training pro-

Table 2. Quantitative results of the Medical Image Fusion. **Bold-face** and underline show the best and second-best values, respectively.

Medical Image Fusion on Harvard Dataset [1]						
	EN \uparrow	SD \uparrow	SF \uparrow	AG \uparrow	SCD \uparrow	SSIM \uparrow
DIF-Net [17]	<u>4.85</u>	52.33	16.53	4.68	1.14	0.26
SDNet [65]	4.23	56.79	<u>28.33</u>	6.98	1.10	0.58
U2Fusion [59]	4.18	52.95	22.02	5.90	1.05	0.54
DeFusion [25]	4.30	63.95	21.15	5.44	1.19	0.76
MATR [53]	4.62	53.35	20.52	5.75	0.40	0.26
CDDFuse [71]	4.41	<u>72.18</u>	28.08	7.26	<u>1.59</u>	0.76
DDFM [72]	4.14	59.12	19.12	4.86	1.36	0.75
GeSeNet [22]	4.76	70.83	28.15	<u>7.54</u>	1.54	0.51
MsgFusion [56]	4.36	69.42	27.98	6.68	1.18	0.51
ReFusion (Ours)	5.08	72.44	28.34	7.59	1.62	<u>0.75</u>

cess, the training images are cropped to 128×128 patches. The batch size was configured to 4, while the hyperparameters α_1 and α_2 are uniformly set to 1. For various image fusion tasks, we describe in detail the datasets used, the comparison methods, and the evaluation metrics applied in different subsections. Computational experiments are executed on a PC with a single NVIDIA GeForce RTX 3090 GPU. Due to space constraints, more visualized comparisons are shown in the supplementary material.

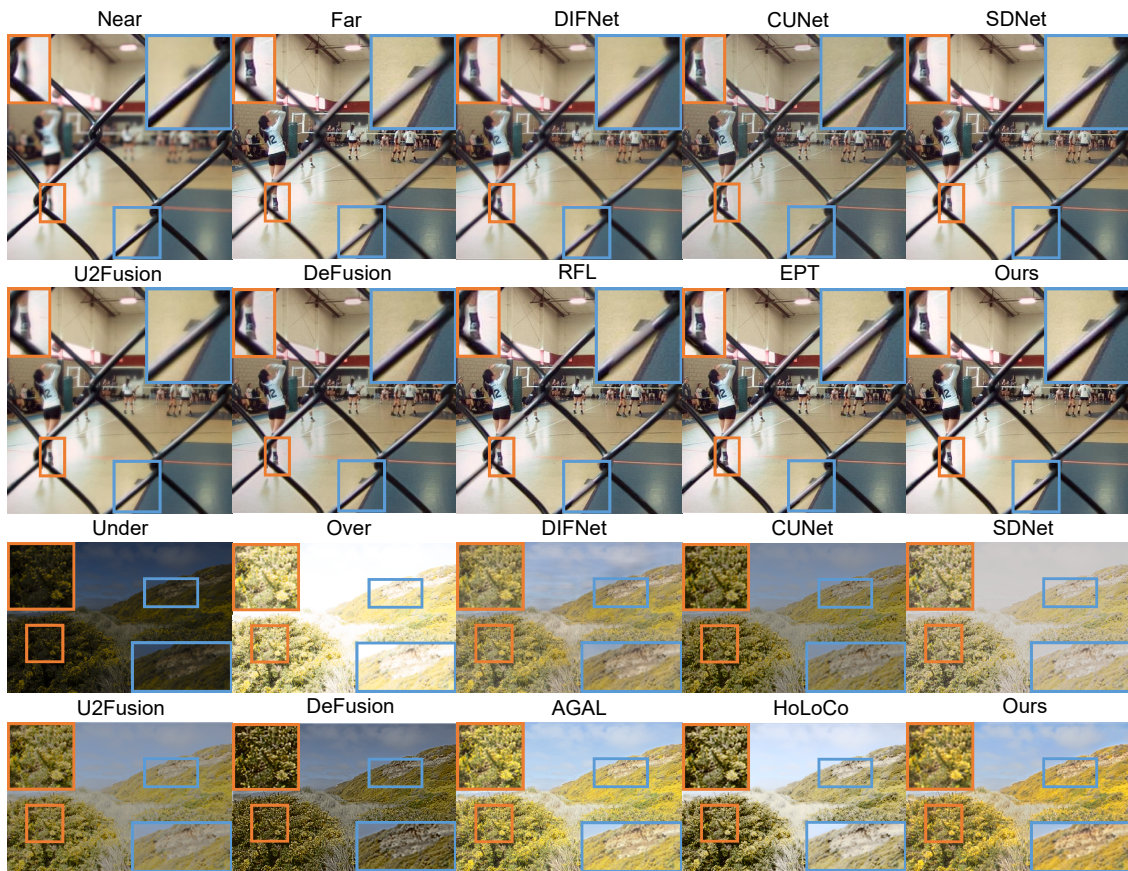


Figure 4. Visual comparison for digital image fusion. The above example is “Lytro_05” in Lytro dataset for multi-focus image fusion and the bottom example is “BloomingGrose” in MEFB dataset for multi-exposure image fusion.

4.2. Multi-modal image fusion

Infrared and Visible Image Fusion. Multi-modal image fusion includes infrared-visible image fusion and medical image fusion. Infrared-visible image fusion experiments are conducted using the MSRS [50] and RoadScene [58] datasets. MSRS comprises 1083 pairs of training images and 361 pairs of test images. We train and test the model on MSRS and further test the generalization ability of the model on 50 pairs of images from RoadScene. We compare our model with several state-of-the-art methods, including SDNet [65], TarDAL [28], DeFusion [25], MetaFusion [69], CDDFuse [71], LRRNet [20], MURF [62], DDFM [72], and SegMIF [30]. Multi-modal image fusion focuses on synthesizing information from different modalities, and in the multi-modal image fusion experiments, we utilize EN, SD, SF, AG, SCD and SSIM to evaluate the fusion performance. we present the quantitative evaluation in Tab. 1. The results demonstrate the superior performance of our approach across six metrics, and emphasize the excellent quality of the fused images produced by our method. Particularly the highest SCD and SSIM indicate

our method’s ability to effectively preserve the complementary information from the source images. The qualitative results, shown in Fig. 2, illustrate that our method is adept at retaining not just the thermal radiation information, but also the intricate texture details. This dual ability to retain both thermal and texture information highlights the adaptability and robustness of our fusion technique.

Medical Image Fusion. We selected 158/50 pairs of images from Harvard dataset [1] as training set/test set containing MRI-CT, MRI-PET, MRI-SPECT image pairs respectively. The contrast methods include DIF-Net [17], SDNet [65], U2Fusion [59], DeFusion [25], MATR [53], CDDFuse [71], DDFM [72], GeSeNet [22], MsgFusion [56]. As shown in Fig. 3, ReFusion successfully retains both the histological information in MRI and also the functional information in PET. The joint retention of the two types of information plays a crucial role in diagnosis and disease monitoring. Qualitative metrics are demonstrated in Tab. 2, where our approach yield excellent results.

Table 3. Quantitative comparison of digital Image Fusion. Best and second-best values are **highlighted** and underlined.

Multi-focus Image Fusion on RealMFF Dataset [50]							Multi-focus Image Fusion on Lytro Dataset [28]						
	EN \uparrow	SD \uparrow	SF \uparrow	VIF \uparrow	Q_{CB} \uparrow	Q_{NCIE} \uparrow		EN \uparrow	SD \uparrow	SF \uparrow	VIF \uparrow	Q_{CB} \uparrow	Q_{NCIE} \uparrow
DIFNet [17]	6.85	48.87	10.98	0.86	0.65	0.83	DIFNet [17]	7.43	52.52	11.47	0.73	0.59	0.83
CUNet [7]	6.58	37.13	13.52	0.74	0.53	0.82	CUNet [7]	7.24	45.78	15.54	0.71	0.57	0.82
SDNet [65]	6.81	49.93	<u>15.58</u>	0.92	0.72	0.83	SDNet [65]	7.47	55.25	16.88	0.84	0.65	0.83
U2Fusion [59]	6.60	47.07	14.35	0.92	0.60	0.82	U2Fusion [59]	7.30	51.95	14.83	0.83	0.64	0.82
DeFusion [25]	<u>6.96</u>	<u>52.84</u>	11.49	<u>0.97</u>	0.71	0.83	DeFusion [25]	7.52	56.65	11.55	0.80	0.62	0.82
RFL [54]	6.87	50.62	15.26	0.95	0.74	<u>0.82</u>	RFL [54]	7.53	57.53	18.43	<u>0.94</u>	<u>0.68</u>	0.83
EPT [55]	6.87	50.64	15.30	0.95	<u>0.75</u>	0.82	EPT [55]	<u>7.53</u>	<u>57.55</u>	<u>18.44</u>	0.94	0.68	0.85
ReFusion (Ours)	6.98	54.35	15.65	1.09	0.76	0.83	ReFusion (Ours)	7.56	59.82	18.56	0.95	0.69	<u>0.83</u>
Multi-exposure Image Fusion on SICE Dataset [6]							Multi-exposure Image Fusion on MEFB Dataset [39]						
	EN \uparrow	SD \uparrow	SF \uparrow	VIF \uparrow	Q_{CB} \uparrow	Q_{NCIE} \uparrow		EN \uparrow	SD \uparrow	SF \uparrow	VIF \uparrow	Q_{CB} \uparrow	Q_{NCIE} \uparrow
DIFNet [17]	6.39	29.11	17.19	0.49	0.26	<u>0.82</u>	DIFNet [17]	7.06	42.62	12.48	0.57	0.37	<u>0.83</u>
CUNet [7]	6.87	32.28	16.22	0.79	0.37	0.81	CUNet [7]	7.14	38.84	12.75	0.71	0.41	0.81
SDNet [65]	6.61	34.94	29.41	0.57	0.44	0.81	SDNet [65]	7.01	48.12	23.60	0.67	0.49	0.82
U2Fusion [59]	6.38	29.30	14.23	0.53	0.36	0.82	U2Fusion [59]	6.89	41.22	13.27	0.60	0.46	0.83
DeFusion [25]	6.61	36.60	16.55	0.77	0.28	0.81	DeFusion [25]	6.91	45.70	13.71	0.67	0.37	0.82
AGAL [29]	<u>7.02</u>	<u>39.70</u>	23.60	0.80	0.38	0.81	AGAL [29]	<u>7.30</u>	<u>52.02</u>	18.53	<u>0.83</u>	0.45	0.83
HoLoCo [32]	6.98	37.07	11.69	0.80	0.40	0.81	HoLoCo [32]	7.24	46.10	13.26	0.76	0.45	0.82
ReFusion (Ours)	7.38	55.48	<u>23.69</u>	1.18	<u>0.41</u>	0.82	ReFusion (Ours)	7.47	62.83	<u>19.01</u>	0.97	<u>0.47</u>	0.83

4.3. Digital Image Fusion

Multi-focus Image Fusion. The main purpose of digital image fusion is to obtain high-quality fused images using multiple source images. In digital image fusion experiments, fusion performance is measured by EN, SD, SF, VIF, Q_{CB} , and Q_{NCIE} . Multi-focus image fusion is performed on two of the most popular datasets, RealMFF [6] and Lytro [39], with 400 pairs of images in RealMFF serving as the training set and 200 pairs of images as the test set. Lytro (20 pairs) is used to verify the generalization performance. The methods compared in the experiments include DIFNet [17], CUNet [7], SDNet [65], U2Fusion [59], DeFusion [25], RFL [54], and EPT [55]. The digital image fusion results displayed in Fig. 4 show that in the multi-focus image fusion, our method succeeds in selecting clear regions in a multi-focus image pair, guaranteeing the clear foreground and background. This is because it is facile to reconstruct unfocused regions using clear fused images, but blurred fused images can greatly increase the difficulty of reconstructing clear regions. ReFusion’s learning scheme forces the network to recognize the difference between clear and blurred. The quantitative results in Tab. 3 demonstrate the excellence of our approach.

Multi-exposure Image Fusion. We perform multi-exposure image fusion experiments on SICE [6] and MEFB [39]. 300 pairs of the SICE are used as training set, simultaneously 100 pairs of SICE and 30 pair of MEFB are used to test and verify generalizability. The comparison methods include DIFNet [17], CUNet [7], SDNet [65], U2Fusion [59], DeFusion [25], AGAL [29], HoLoCo [32]. The quantitative and qualitative results demonstrate that ReFusion can successfully process multiple images with different exposures, extend the dynamic range of the image,

Table 4. Ablation experiment results of infrared-visible image fusion. **Bold** indicates the best value.

Configurations		EN	SD	SF	AG	SCD	SSIM
I	Fixed W and V as $1/2$	6.26	37.49	10.86	2.69	1.42	0.37
II	$I_f = W_a * I_a + W_b * I_b$	6.32	38.42	11.03	2.89	1.43	0.42
III	AFM \rightarrow Concatenate	6.47	39.26	10.93	1.46	2.94	0.39
IV	w/o Interactive feature extraction	6.52	39.25	10.96	1.54	3.01	0.49
V	w/o Gating Feature Refinement	6.55	39.53	10.93	1.62	2.98	0.48
Ours		6.71	42.89	11.64	3.80	1.67	0.51

but also enhance the image quality and the contrast.

4.4. Learnable Loss

Our method parameterizes the fusion loss and utilizes a loss proposal network to predict its intensity and gradient trade-off between the source images. The process of variation of W and V during training and the training results on different fusion tasks will be further shown in the supplementary material.

4.5. Ablation Studies

We take infrared visible image fusion as an example to conduct ablation experiments to verify the rationality of the module, and the results are shown in Tab. 4. In Exp. I, we abandon the learnability of fusion loss and fix W and V constant to $1/2$ to train the fusion network. In Exp. II, we change the fusion module to decision-based fusion and train like ReFusion. We make the changes of changing AFM to Concatenate, removing the interaction extraction module, and removing the gating refinement module in In Exp. III-Exp. V, respectively. Rational ablation experiments justify the experimental setup.

5. Conclusion

In this paper, we propose a unified image fusion algorithm based on meta-learning, where the loss proposal module proposes the loss function for training the fusion module. The loss proposal module is updated by the reconstruction loss in a meta-learning manner. The algorithm learns how to fuse from the reconstruction task and applies to a variety of image fusion tasks. It can solve the natural difficulty of the lack of ground truth for image fusion tasks that require manual design of the loss function. Experiments on different fusion tasks demonstrate that our method can perform multiple fusion tasks, including multi-modal, multi-focus, and multi-exposure image fusion tasks with high quality.

References

- [1] Harvard medical website. <http://www.med.harvard.edu/AANLIB/home.html>. 6, 7
- [2] Antreas Antoniou and Amos J. Storkey. Learning to learn by self-critique. In *NeurIPS*, pages 9936–9946, 2019. 3
- [3] Sungyong Baik, Janghoon Choi, Heewon Kim, Dohee Cho, Jaesik Min, and Kyoung Mu Lee. Meta-learning with task-adaptive loss function for few-shot learning. In *ICCV*, pages 9445–9454. IEEE, 2021. 3
- [4] Wele Gedara Chaminda Bandara and Vishal M. Patel. Hypertransformer: A textural and spectral feature fusion transformer for pansharpening. In *Proceedings of the IEEE/CVF Conference on Computer Vision and Pattern Recognition (CVPR)*, pages 1757–1767, 2022. 1
- [5] D.M. Bulanon, T.F. Burks, and V. Alchanatis. Image fusion of visible and thermal images for fruit detection. *Biosystems Engineering*, 103(1):12–22, 2009. 2
- [6] Jianrui Cai, Shuhang Gu, and Lei Zhang. Learning a deep single image contrast enhancer from multi-exposure images. *IEEE Transactions on Image Processing*, 27(4):2049–2062, 2018. 8
- [7] Xin Deng and Pier Luigi Dragotti. Deep convolutional neural network for multi-modal image restoration and fusion. *IEEE transactions on pattern analysis and machine intelligence*, 43(10):3333–3348, 2020. 8
- [8] Vakaimalar E, Mala K, and Suresh Babu R. Multifocus image fusion scheme based on discrete cosine transform and spatial frequency. *Multim. Tools Appl.*, 78(13):17573–17587, 2019. 2
- [9] Chelsea Finn, Pieter Abbeel, and Sergey Levine. Model-agnostic meta-learning for fast adaptation of deep networks. In *International conference on machine learning*, pages 1126–1135. PMLR, 2017. 2, 3
- [10] Chelsea Finn, Aravind Rajeswaran, Sham Kakade, and Sergey Levine. Online meta-learning. In *International Conference on Machine Learning*, pages 1920–1930. PMLR, 2019. 3
- [11] Timothy M. Hospedales, Antreas Antoniou, Paul Micaelli, and Amos J. Storkey. Meta-learning in neural networks: A survey. *IEEE Trans. Pattern Anal. Mach. Intell.*, 44(9):5149–5169, 2022. 2
- [12] Rein Houthoofd, Yuhua Chen, Phillip Isola, Bradly C. Stadie, Filip Wolski, Jonathan Ho, and Pieter Abbeel. Evolved policy gradients. In *NeurIPS*, pages 5405–5414, 2018. 3
- [13] Xingyu Hu, Junjun Jiang, Xianming Liu, and Jiayi Ma. Zmf: Zero-shot multi-focus image fusion. *Information Fusion*, 92:127–138, 2023. 1
- [14] Zhanbo Huang, Jinyuan Liu, Xin Fan, Risheng Liu, Wei Zhong, and Zhongxuan Luo. Reconet: Recurrent correction network for fast and efficient multi-modality image fusion. In *European Conference on Computer Vision*, pages 539–555. Springer, 2022. 2
- [15] Alex Pappachen James and Belur V. Dasarathy. Medical image fusion: A survey of the state of the art. *Information Fusion*, 19:4–19, 2014. 1
- [16] Xin Jin, Qian Jiang, Shaowen Yao, Dongming Zhou, Ren-can Nie, Shin-Jye Lee, and Kangjian He. Infrared and visual image fusion method based on discrete cosine transform and local spatial frequency in discrete stationary wavelet transform domain. *Infrared Physics & Technology*, 88:1–12, 2018. 2
- [17] Hyungjoo Jung, Youngjung Kim, Hyunsung Jang, Namkoo Ha, and Kwanghoon Sohn. Unsupervised deep image fusion with structure tensor representations. *IEEE Transactions on Image Processing*, 29:3845–3858, 2020. 6, 7, 8
- [18] Hui Li and Xiao-Jun Wu. Densefuse: A fusion approach to infrared and visible images. *IEEE Transactions on Image Processing*, 28(5):2614–2623, 2018. 2
- [19] Hui Li, Xiao-Jun Wu, and Josef Kittler. Rfn-nest: An end-to-end residual fusion network for infrared and visible images. *Information Fusion*, 73:72–86, 2021. 2
- [20] Hui Li, Tianyang Xu, Xiao-Jun Wu, Jiwen Lu, and Josef Kittler. Lrrnet: A novel representation learning guided fusion network for infrared and visible images. *IEEE transactions on pattern analysis and machine intelligence*, 2023. 6, 7
- [21] Jiawei Li, Jinyuan Liu, Shihua Zhou, Qiang Zhang, and Nikola K. Kasabov. Gesenet: A general semantic-guided network with couple mask ensemble for medical image fusion. *IEEE Transactions on Neural Networks and Learning Systems*, pages 1–14, 2023. 1
- [22] Jiawei Li, Jinyuan Liu, Shihua Zhou, Qiang Zhang, and Nikola K Kasabov. Gesenet: A general semantic-guided network with couple mask ensemble for medical image fusion. *IEEE Transactions on Neural Networks and Learning Systems*, 2023. 6, 7
- [23] Yuqi Li, Haitao Zhao, Zhengwei Hu, Qianqian Wang, and Yuru Chen. Ivfusenet: Fusion of infrared and visible light images for depth prediction. *Inf. Fusion*, 58:1–12, 2020. 1
- [24] Zhenguo Li, Fengwei Zhou, Fei Chen, and Hang Li. Meta-sgd: Learning to learn quickly for few-shot learning. *arXiv preprint arXiv:1707.09835*, 2017. 2, 3
- [25] Pengwei Liang, Junjun Jiang, Xianming Liu, and Jiayi Ma. Fusion from decomposition: A self-supervised decomposition approach for image fusion. In *ECCV*, 2022. 2, 6, 7, 8
- [26] Geert Litjens, Thijs Kooi, Babak Ehteshami Bejnordi, Arnaud Arindra Adiyoso Setio, Francesco Ciompi, Mohsen Ghafoorian, Jeroen Awm Van Der Laak, Bram Van Ginneken, and Clara I Sánchez. A survey on deep learning in

- medical image analysis. *Medical Image Analysis*, 42:60–88, 2017. 1
- [27] Hanxiao Liu, Karen Simonyan, and Yiming Yang. DARTS: differentiable architecture search. *CoRR*, abs/1806.09055, 2018. 2
- [28] Jinyuan Liu, Xin Fan, Zhanbo Huang, Guanyao Wu, Risheng Liu, Wei Zhong, and Zhongxuan Luo. Target-aware dual adversarial learning and a multi-scenario multi-modality benchmark to fuse infrared and visible for object detection. In *CVPR*, pages 5792–5801, 2022. 2, 6, 7, 8
- [29] Jinyuan Liu, Jingjie Shang, Risheng Liu, and Xin Fan. Attention-guided global-local adversarial learning for detail-preserving multi-exposure image fusion. *IEEE Transactions on Circuits and Systems for Video Technology*, 32(8):5026–5040, 2022. 8
- [30] Jinyuan Liu, Zhu Liu, Guanyao Wu, Long Ma, Risheng Liu, Wei Zhong, Zhongxuan Luo, and Xin Fan. Multi-interactive feature learning and a full-time multi-modality benchmark for image fusion and segmentation. *CoRR*, abs/2308.02097, 2023. 6, 7
- [31] Jinyuan Liu, Zhu Liu, Guanyao Wu, Long Ma, Risheng Liu, Wei Zhong, Zhongxuan Luo, and Xin Fan. Multi-interactive feature learning and a full-time multi-modality benchmark for image fusion and segmentation. In *Proceedings of the IEEE/CVF International Conference on Computer Vision (ICCV)*, pages 8115–8124, 2023. 2
- [32] Jinyuan Liu, Guanyao Wu, Junsheng Luan, Zhiying Jiang, Risheng Liu, and Xin Fan. Holoco: Holistic and local contrastive learning network for multi-exposure image fusion. *Information Fusion*, 95:237–249, 2023. 8
- [33] Risheng Liu, Zhu Liu, Jinyuan Liu, and Xin Fan. Searching a hierarchically aggregated fusion architecture for fast multi-modality image fusion. In *ACM Multimedia*, pages 1600–1608. ACM, 2021. 3
- [34] Xingbin Liu, Wenbo Mei, and Huiqian Du. Structure tensor and nonsubsampling shearlet transform based algorithm for CT and MRI image fusion. *Neurocomputing*, 235:131–139, 2017. 2
- [35] Yipeng Liu, Jing Jin, Qiang Wang, Yi Shen, and Xiaoqi Dong. Region level based multi-focus image fusion using quaternion wavelet and normalized cut. *Signal Process.*, 97: 9–30, 2014. 2
- [36] Yu Liu, Lei Wang, Huafeng Li, and Xun Chen. Multi-focus image fusion with deep residual learning and focus property detection. *Information Fusion*, 86:1–16, 2022. 1
- [37] Jiayi Ma, Wei Yu, Pengwei Liang, Chang Li, and Junjun Jiang. FusionGAN: A generative adversarial network for infrared and visible image fusion. *Information Fusion*, 48:11–26, 2019. 1, 2
- [38] Jiayi Ma, Han Xu, Junjun Jiang, Xiaoguang Mei, and Xiaoping Zhang. DdGAN: A dual-discriminator conditional generative adversarial network for multi-resolution image fusion. *IEEE Transactions on Image Processing*, 29:4980–4995, 2020. 1
- [39] Kede Ma, Hui Li, Hongwei Yong, Zhou Wang, Deyu Meng, and Lei Zhang. Robust multi-exposure image fusion: A structural patch decomposition approach. *IEEE Transactions on Image Processing*, 26(5):2519–2532, 2017. 1, 8
- [40] Kede Ma, Zhengfang Duanmu, Hanwei Zhu, Yuming Fang, and Zhou Wang. Deep guided learning for fast multi-exposure image fusion. *IEEE Transactions on Image Processing*, 2020. 1
- [41] Vivek Maik, Dohee Cho, Jeongho Shin, and Joon Ki Paik. Regularized restoration using image fusion for digital auto-focusing. *IEEE Trans. Circuits Syst. Video Technol.*, 17(10): 1360–1369, 2007. 1
- [42] Alex Nichol, Joshua Achiam, and John Schulman. On first-order meta-learning algorithms. *CoRR*, abs/1803.02999, 2018. 3
- [43] Xinran Qin, Yuhui Quan, Tongyao Pang, and Hui Ji. Ground-truth free meta-learning for deep compressive sampling. In *CVPR*, pages 9947–9956. IEEE, 2023. 3
- [44] Mengye Ren, Wenyuan Zeng, Bin Yang, and Raquel Urtasun. Learning to reweight examples for robust deep learning. In *ICML*, pages 4334–4343. PMLR, 2018. 3
- [45] Jun Shu, Qi Xie, Lixuan Yi, Qian Zhao, Sanping Zhou, Zongben Xu, and Deyu Meng. Meta-weight-net: Learning an explicit mapping for sample weighting. *NIPS*, 32, 2019. 3
- [46] Yiming Sun, Bing Cao, Pengfei Zhu, and Qinghua Hu. Det-fusion: A detection-driven infrared and visible image fusion network. In *Proceedings of the ACM International Conference on Multimedia (ACM MM)*, pages 4003–4011, 2022. 2
- [47] Linfeng Tang, Yuxin Deng, Yong Ma, Jun Huang, and Jiayi Ma. Superfusion: A versatile image registration and fusion network with semantic awareness. *IEEE/CAA Journal of Automatica Sinica*, 9(12):2121–2137, 2022. 2
- [48] Linfeng Tang, Jiteng Yuan, and Jiayi Ma. Image fusion in the loop of high-level vision tasks: A semantic-aware real-time infrared and visible image fusion network. *Information Fusion*, 82:28–42, 2022. 2
- [49] Linfeng Tang, Jiteng Yuan, and Jiayi Ma. Image fusion in the loop of high-level vision tasks: A semantic-aware real-time infrared and visible image fusion network. *Information Fusion*, 82:28–42, 2022. 2
- [50] Linfeng Tang, Jiteng Yuan, Hao Zhang, Xingyu Jiang, and Jiayi Ma. Piafusion: A progressive infrared and visible image fusion network based on illumination aware. *Inf. Fusion*, 83-84:79–92, 2022. 6, 7, 8
- [51] Linfeng Tang, Jiteng Yuan, Hao Zhang, Xingyu Jiang, and Jiayi Ma. Piafusion: A progressive infrared and visible image fusion network based on illumination aware. *Information Fusion*, 83:79–92, 2022. 1, 2
- [52] Linfeng Tang, Hao Zhang, Han Xu, and Jiayi Ma. Rethinking the necessity of image fusion in high-level vision tasks: A practical infrared and visible image fusion network based on progressive semantic injection and scene fidelity. *Information Fusion*, page 101870, 2023. 2
- [53] Wei Tang, Fazhi He, Yu Liu, and Yansong Duan. Matr: Multimodal medical image fusion via multiscale adaptive transformer. *IEEE Transactions on Image Processing*, 31:5134–5149, 2022. 6, 7
- [54] Zeyu Wang, Xiongfei Li, Haoran Duan, and Xiaoli Zhang. A self-supervised residual feature learning model for multifocus image fusion. *IEEE Transactions on Image Processing*, 31:4527–4542, 2022. 1, 8

- [55] Zeyu Wang, Xiongfei Li, Libo Zhao, Haoran Duan, Shidong Wang, Hao Liu, and Xiaoli Zhang. When multi-focus image fusion networks meet traditional edge-preservation technology. *International Journal of Computer Vision*, pages 1–24, 2023. [8](#)
- [56] Jinyu Wen, Feiwei Qin, Jiao Du, Meie Fang, Xinhua Wei, CL Philip Chen, and Ping Li. Msgfusion: Medical semantic guided two-branch network for multimodal brain image fusion. *IEEE Transactions on Multimedia*, 2023. [6](#), [7](#)
- [57] Han Xu and Jiayi Ma. Emfusion: An unsupervised enhanced medical image fusion network. *Information Fusion*, 76:177–186, 2021. [1](#)
- [58] Han Xu, Jiayi Ma, Zhuliang Le, Junjun Jiang, and Xiaojie Guo. Fusiondn: A unified densely connected network for image fusion. In *AAAI*, pages 12484–12491, 2020. [6](#), [7](#)
- [59] Han Xu, Jiayi Ma, Junjun Jiang, Xiaojie Guo, and Haibin Ling. U2fusion: A unified unsupervised image fusion network. *IEEE TPAMI*, 44(1):502–518, 2022. [6](#), [7](#), [8](#)
- [60] Han Xu, Jiayi Ma, Junjun Jiang, Xiaojie Guo, and Haibin Ling. U2fusion: A unified unsupervised image fusion network. *IEEE Trans. Pattern Anal. Mach. Intell.*, 44(1):502–518, 2022. [2](#), [3](#)
- [61] Han Xu, Jiayi Ma, Jiteng Yuan, Zhuliang Le, and Wei Liu. Rfnnet: Unsupervised network for mutually reinforcing multimodal image registration and fusion. In *Proceedings of the IEEE/CVF conference on computer vision and pattern recognition*, pages 19679–19688, 2022. [2](#)
- [62] Han Xu, Jiteng Yuan, and Jiayi Ma. Murf: Mutually reinforcing multi-modal image registration and fusion. *IEEE Transactions on Pattern Analysis and Machine Intelligence*, 2023. [6](#), [7](#)
- [63] Shuang Xu, Jiangshe Zhang, Zixiang Zhao, Kai Sun, Junmin Liu, and Chunxia Zhang. Deep gradient projection networks for pan-sharpening. In *Proceedings of the IEEE/CVF Conference on Computer Vision and Pattern Recognition (CVPR)*, pages 1366–1375, 2021. [1](#)
- [64] Syed Waqas Zamir, Aditya Arora, Salman H. Khan, Munawar Hayat, Fahad Shahbaz Khan, and Ming-Hsuan Yang. Restormer: Efficient transformer for high-resolution image restoration. *CoRR*, abs/2111.09881, 2021. [5](#)
- [65] Hao Zhang and Jiayi Ma. Sdnet: A versatile squeeze-and-decomposition network for real-time image fusion. *Int. J. Comput. Vis.*, 129(10):2761–2785, 2021. [1](#), [2](#), [6](#), [7](#), [8](#)
- [66] Xingchen Zhang. Benchmarking and comparing multi-exposure image fusion algorithms. *Information Fusion*, 74: 111–131, 2021. [1](#)
- [67] Xingchen Zhang. Deep learning-based multi-focus image fusion: A survey and a comparative study. *IEEE Transactions on Pattern Analysis and Machine Intelligence*, 44(9): 4819–4838, 2021. [1](#)
- [68] Wenda Zhao, Shigeng Xie, Fan Zhao, You He, and Huchuan Lu. Metafusion: Infrared and visible image fusion via meta-feature embedding from object detection. In *CVPR*, pages 13955–13965. IEEE, 2023. [2](#), [3](#)
- [69] Wenda Zhao, Shigeng Xie, Fan Zhao, You He, and Huchuan Lu. Metafusion: Infrared and visible image fusion via meta-feature embedding from object detection. In *Proceedings of the IEEE/CVF Conference on Computer Vision and Pattern Recognition*, pages 13955–13965, 2023. [6](#), [7](#)
- [70] Zixiang Zhao, Shuang Xu, Chunxia Zhang, Junmin Liu, Pengfei Li, and Jianshe Zhang. Didfuse: Deep image decomposition for infrared and visible image fusion. *arXiv preprint arXiv:2003.09210*, 2020. [1](#), [2](#)
- [71] Zixiang Zhao, Haowen Bai, Jianshe Zhang, Yulun Zhang, Shuang Xu, Zudi Lin, Radu Timofte, and Luc Van Gool. Cddfuse: Correlation-driven dual-branch feature decomposition for multi-modality image fusion. In *Proceedings of the IEEE/CVF Conference on Computer Vision and Pattern Recognition*, pages 5906–5916, 2023. [2](#), [6](#), [7](#)
- [72] Zixiang Zhao, Haowen Bai, Yuanzhi Zhu, Jianshe Zhang, Shuang Xu, Yulun Zhang, Kai Zhang, Deyu Meng, Radu Timofte, and Luc Van Gool. DDFM: denoising diffusion model for multi-modality image fusion. *CoRR*, abs/2303.06840, 2023. [2](#), [6](#), [7](#)
- [73] Huabing Zhou, Wei Wu, Yanduo Zhang, Jiayi Ma, and Haibin Ling. Semantic-supervised infrared and visible image fusion via a dual-discriminator generative adversarial network. *IEEE Transactions on Multimedia*, 2021. [2](#)